Time evolution of deformation in a human cartilage under cyclic loading

Lihai Zhang

Department of Infrastructure Engineering, The University of Melbourne, VIC 3010, Australia

Tel: +(613) 83447179; Fax: +(613) 83444616; Email: lihzhang@unimelb.edu.au

Saeed Miramini

Department of Infrastructure Engineering, The University of Melbourne, Victoria 3010, Australia

Tel: +61 469754951; Email: miramini@pgrad.unimelb.edu.au

David W. Smith

Faculty of Engineering, Computing and Mathematics, The University of Western Australia, WA, 6009, Australia

Tel: +(618) 6488 5531; Fax: +(618) 6488 1089; Email: david.smith@uwa.edu.au

Bruce S. Gardiner

Faculty of Engineering, Computing and Mathematics, The University of Western Australia, WA, 6009, Australia

Tel: +(618) 6488 1537; Fax: +(618) 6488 1089; Email: bruce.gardiner@uwa.edu.au

Alan J. Grodzinsky

Center for Biomedical Engineering and Departments of Biological Engineering, Electrical Engineering and Computer Science, and Mechanical Engineering, Massachusetts Institute of Technology, Cambridge, Massachusetts, USA.

Tel: +(617) 253-4969; Fax: (617) 258-5239; Email: alg@mit.edu

Abstract - Recent imaging has revealed that *in vivo* contact deformations of human knee cartilage under physiological loadings are surprisingly large—typically on the order of 10%, but up to 20% or 30% of tibiofemora cartilage thickness depending on loading conditions. In this paper we develop a biphasic, large deformation, non-linear poroelastic model of cartilage that can accurately represent the time dependence and magnitude of cyclic cartilage deformations *in vivo*. The model takes into account cartilage tension-compression nonlinearity and a new constitutive relation in which the compressive stiffness and hydraulic permeability of the cartilage adjusts in response to the strain-dependent aggrecan concentration. The model predictions are validated using experimental test results on osteochondral plugs obtained from human cadavers. We find that model parameters can be optimised to give an excellent fit to the experimental data. Using typical hydraulic conductivity and stiffness parameters for healthy cartilage, we find that the experimentally observed transient and steady state tissue deformations under cyclic loading and unloading can be reproduced by the model. Steady state tissue deformations are shown to cycle between 10% (exudation strain) and 20% (total strain) in response to the cyclic test loads. At steady-state cyclic loading, the pore fluid exuded from the tissue is exactly equal to the pore fluid imbibed by the tissue during each load cycle.

Key Words - Cartilage; Aggrecan; Computational modelling; Large deformation; Exudation strain; Compressive stiffness; Permeability

INTRODUCTION

The primary function of cartilage is to protect articulating joints from damage and wear under the large contact forces experienced during daily physical activities. The ability of cartilage to maintain its physiological function in this hostile mechanical environment depends on the tissue's ability to avoid excessive tissue strain, extracellular matrix (ECM) degradation and cell death. In cartilage this seems to be achieved by linking appropriate ECM biosynthesis to tissue deformation[3]. Dynamic compression of cartilage induces deformation of chondrocytes, gradients in hydrostatic pressure and corresponding intra-tissue fluid flow, which together stimulate ECM biosynthesis (and consequently changes tissue osmotic swelling pressure and thereby tissue resistance to compression)[2; 8; 17-19; 40]. Further, interstitial fluid flow resulting from dynamic loading also plays a role in the transport behaviour of solutes (*e.g.* insulin-like growth factors, glucose, oxygen, etc.) within the tissue[15; 16; 52; 54-57; 59; 60].

The mechanical behaviour of cartilage is largely determined by the interactions between interstitial fluid, the proteoglycan aggrecan and Type II collagen[18]. Approximately 10%-30% of cartilage's dry weight is proteoglycan [36]. Aggrecan is a major component of the cartilage ECM (MW ~1-3 MDa)[20]. Up to 100 aggrecan molecules can bind to hyaluronic acid, and once stabilized by link protein, forms huge polymers known as aggregate (>200 MDa). Each aggrecan monomer contains up to ~100 highly negatively charged chondroitin sulfate glycosaminoglycan (GAG) chains that attract counter ions within the tissue[31], thereby generating an osmotic pressure that contributes significantly to the equilibrium compressive stiffness of cartilage [9; 14; 30; 49]. Further, the densely packed GAG chains provide the principal resistance to intra-tissue fluid flow. The aggrecan content normally increases from the superficial zone to deep zone, which contributes to the depth-dependent inhomogeneity in the mechanical properties of cartilage[49].

About two-thirds of the dry weight of adult articular cartilage is collagen. The heteropolymeric type II/IX/XI collagen fibrils forms a cross-banded network throughout cartilage, providing the main contribution to cartilage's tensile and shear strength[50]. The collagen network within cartilage is in a state of tensile prestress, and it constrains the loss of aggrecan from the matrix[4523]. Net loss of aggrecan from the collagen network (via proteolytic and/or advective and diffusive transport mechanisms), causes the cartilage to undergo excessive deformation, which further increases cartilage degradation and wear with use[28] (i.e., aggrecan loss has a direct mechanical effect on matrix integrity). When the joint can no longer function properly, as determined by clinical criteria, it is said to be diseased.

In the cartilage superficial zone, the collagen fibrils are densely packed and oriented parallel to the articular surface; the aggrecan content is low. In the middle zone, the collagen is more randomly oriented and the aggrecan content increases. In the deep zone, the collagen fibrils are larger and are typically oriented perpendicular to the articular surface, and the aggrecan content reaches a maximum [44; 45]. Thus, as with aggrecan, the composition and spatial arrangement of collagen helps define the heterogeneous mechanical behaviour of cartilage.

The rate of fluid flow exiting the cartilage surface is strongly correlated to the degree of deformation caused by dynamic loading. To study the load-deformation response of cartilage in detail, Barker and Seedhom (2001) [3] applied cyclic loading to osteochndral plugs taken from human cadaveric knees. Under controlled laboratory conditions, they applied loads to the surface of the cartilage using a plane-ended impervious indenter 3 mm in diameter. Based on the measurement of 'total' and 'exudation' strains during loading and recovery phases of each cycle, they proposed an empirical viscoelastic model to estimate the time-dependent total and exudation strains assuming a constant Young's modulus for the cartilage. The difficulty with viscoelastic models of poroelastic phenomena is that the

parameters estimated for the constitutive law are problem specific (they are not true material properties tied back to ECM content), and so the parameters cannot be used for different geometries, boundary conditions or material properties. Our overall objective is to develop a parsimonious, non-linear poroelastic model to interpret the experimental data for these human cartilage samples.

Many computational models of articular cartilage attempt to capture the experimentally observed deformation behaviour of cartilage using a constant (equilibrium) Young's modulus and permeability[32; 46]. Unfortunately these models have limited capability for capturing the tissue response to a variety of loading conditions, because it is known that both the compression and permeability response of cartilage are actually highly non-linear. The problem is further complicated due to the fact that cartilage exhibits a so-called "tension-compression nonlinearity" behaviour[6; 24; 46; 53]. Experimental studies have shown a linear relationship on a log-log plot between cartilage permeability and the aggrecan volume fraction [51]. Most importantly, by using a constant aggregate modulus and permeability, these conventional models may not be able to provide a realistic prediction of the large deformation response of cartilage tissue subject to external cyclic loading.

Many sophisticated models capturing various aspects of cartilage behaviour have been proposed (e.g. biphasic [12; 35; 47], triphasic [1; 26; 48], quadri-phasic [29] models). However, we believe there is a need for a simplified biphasic model that can be used to give a reasonably accurate approximation to the time evolution of the strain state within full thickness cartilage under low frequency cyclic loads, as experienced during activities such as running and walking. Bearing in mind that cartilage is a dynamic living tissue that is continually damaged and repaired (and so there is a need to include extracellular matrix turnover in future models), this model was purposefully designed to be a balance between accuracy, flexibility (i.e. so the

model can be calibrated against test measurements made on human cadaver specimens) and tractability.

To overcome the limitations of a constant cartilage Young's modulus, constant cartilage permeability and to account for large deformations, in this study we introduce a new constitutive relation in our poroelastic model, which links the compressive stiffness and permeability to aggrecan volume fraction via the volumetric strain of the tissue. Further, the significant difference in magnitude between the cartilage stiffness in tension and compression is also included in the model. In the following, critical model parameters are indentified by calibration against the experimental results of Barker et al. (2001) [3]. The model is then used to investigate the large deformation behaviour of human osteochondral plugs under cyclic loads.

Here we note that the applicability of this model is restricted to a constant isotonic salt concentration bathing the cartilage tissue (i.e. the salt concentration found under physiological conditions). In practice this restriction is not significant because *in vivo*, the salt concentration of the blood (and by extension the synovial fluid) is very closely controlled by the kidney, and so may reasonably be assumed to be invariant. To ensure that the entropy inequality is maintained at all times, we also require that the matrix of coefficients relating hydraulic flow to fluid pressure and electrokinetic fluxes to a voltage, together with their 'cross-coefficients', must be of positive-definite quadratic form and so satisfy Onsager's entropy inequality requirements. With these qualifications the model is thermodynamically admissible. Should ion migration processes be of interest to an investigator, then a more appropriate fully coupled theory should be employed (e.g., a fully coupled phenomenological theory or quadriphasic theory [29]).

The research outcome of the current study shows that a realistic non-linear constitutive model within a poroelastic framework can replicate human cadaver data involving large deformations using a relatively simple biphasic model. The simplicity of this model provides a tractable computational model that can be expanded in the future to incorporate reactive-transport of many different molecules together with the homeostatic processes known to be important for maintaining healthy cartilage.

MATERIALS AND METHODS

In this study, we wish to reproduce the experimentally observed deformation behaviour of osteochondral plugs obtained from cadaveric knees. The test specimens were subjected to cyclic loading, comparable in load magnitude and frequency to that experienced during walking, delivered using a specialized indentation apparatus (Figure 1) [3]. The hemispherical or flat indenter used in the testing can be treated as an axisymmetric loading on the surface of the cartilage. The biomechanical behaviour of cartilage is modelled using the theory of porous media[37; 38; 54; 55; 58]. A particular constituent of fluid-filled cartilage tissue is considered occupies a domain Ω_0^α , i.e. solid phase ($\alpha = s$) or fluid phase ($\alpha = f$). The sum of volume fraction of solid phase (ϕ^s) and volume fraction of fluid phase (ϕ^f) must satisfy $\phi^s + \phi^f = 1$. The time-dependent position of the particle in the current Eulerian configuration Ω_t is given by

$$x\left(X^\alpha, t\right) = X^\alpha + u^\alpha\left(X^\alpha, t\right) \tag{1}$$

where X^α is the position of the α - constituent in material coordinates and u^α is the α - constituent displacement.

Conservation of mass

Conservation of mass of the solid phase and fluid phase leads to [54]

$$\nabla \bullet \left[\phi^f \left(\mathbf{v}^{\mathrm{f}} - \mathbf{v}^{\mathrm{s}}\right)\right] + \nabla \bullet \mathbf{v}^{\mathrm{s}} = 0 \qquad (2)$$

where $\mathbf{v}^{\mathbf{s}}$ and $\mathbf{v}^{\mathbf{f}}$ are the velocity of solid and fluid phase respectively, and $\nabla \bullet$ denotes the divergence operator.

Conservation of momentum

Ignoring the body and inertial forces, the momentum equation of the solid phase is given by

$$\nabla \bullet \boldsymbol{\sigma}^{\alpha} + \pi^{\alpha} = 0 \qquad 3)$$

where σ^{α} is the Cauchy stress tensor for the α -constituent and π^{α} is the momentum exchange between the phases. Again assuming intrinsically incompressible constituents, the Cauchy stress tensors of the solid and fluid phases are defined as

$$\boldsymbol{\sigma}^{\mathbf{s}} = -\phi^{\mathbf{s}} p\mathbf{I} + \boldsymbol{\sigma}_{\mathbf{E}}^{\mathbf{s}} \qquad (4)$$

$$\boldsymbol{\sigma}^{\mathbf{f}} = -\phi^{\mathbf{f}} p\mathbf{I} \qquad (5)$$

where $\boldsymbol{\sigma}_{\mathbf{E}}^{\mathbf{s}}$ is the incremental elastic stress resulting from solid deformation due to loading, $\mathbf{I}$ is the identity tensor and p is incremental interstitial fluid pressure. The solid constituent stress in spatial coordinates (i.e. the Cauchy stress) is given by

$$\boldsymbol{\sigma}_{\mathbf{E}}^{\mathbf{s}} = \frac{1}{J^s}\mathbf{F}^{\mathbf{s}} \bullet 2\frac{\partial U\left(\mathbf{u}^{\mathbf{s}}\right)}{\partial \mathbf{C}^{\mathbf{s}}} \bullet \mathbf{F}^{\mathbf{s}^{\mathrm{T}}} \qquad (6)$$

where $U\left(\mathbf{u}^{\mathbf{s}}\right)$ is the Helmholtz energy per unit reference volume stored in the solid (i.e. the strain energy density), $\mathbf{F}^{\mathbf{s}}$ is the deformation gradient of the solid phase, $\mathbf{C}^{\mathbf{s}} = \mathbf{F}^{\mathbf{s}^{\mathrm{T}}} \bullet \mathbf{F}^{\mathbf{s}}$ is the right Cauchy-Green deformation tensor of the solid phase, and $J^s = \det \mathbf{F}^{\mathbf{s}}$ is the volume change of solid phase.

Darcy's law

By defining all fluid quantities with respect to the solid phase, we obtain

$$\dot{\mathbf{W}} + \mathbf{k} \bullet \nabla_0 p = 0 \tag{7}$$

where ∇_0 is the material gradient operator on Ω_0^s, $\mathbf{k}$ is the Lagrangian permeability tensor, and $\dot{\mathbf{W}}$ the Lagrangian fluid velocity relative to the solid phase, that is the material time derivative of Lagrangian relative fluid displacement $\mathbf{W}$, which is defined as

$$\dot{\mathbf{W}} = J^s \mathbf{F}^{\mathbf{s}-1} \bullet \left[\phi^f \left(\mathbf{v}^{\mathbf{f}} - \mathbf{v}^{\mathbf{s}} \right) \right] \tag{8}$$

In addition, the Lagrangian permeability tensor is given by

$$\mathbf{k} = J^s \mathbf{F}^{\mathbf{s}-1} \bullet \boldsymbol{\kappa} \bullet \mathbf{F}^{\mathbf{s}-t} \tag{9}$$

Tension-compression behaviour of cartilage ECM

Experimental studies have shown that cartilage responds differently in tension and compression, and exhibits a so-called "tension-compression nonlinearity" behaviour [6; 24; 46]. Soltz and Ateshian (2000) [46] proposed that the mechanical behaviour of cartilage's solid phase can be described by the "orthotropic octant-wise linear elasticity" model of Curnier et al. (1995) [11]. Thus, the elastic stress $\boldsymbol{\sigma}_{\mathbf{E}}^{\mathbf{s}}$ resulting from solid phase deformation in Equation (4) is replaced by

$$\sigma_E^s = \sum_{a=1}^{3} \left\{ \lambda_1 \left[\mathbf{A}_a : \mathbf{E} \right] \mathrm{tr}\left(\mathbf{A}_a \mathbf{E} \right) \mathbf{A}_a + \sum_{\substack{b=1 \\ b \neq a}}^{3} \lambda_2 \mathrm{tr}\left(\mathbf{A}_a \mathbf{E} \right) \mathbf{A}_b \right\} + 2\mu \mathbf{E} \tag{10}$$

$$\lambda_1 \left[\mathbf{A}_a : \mathbf{E} \right] = \begin{cases} \lambda_{-1}, & \mathbf{A}_a : \mathbf{E} < \mathbf{0} \\ \lambda_{+1}, & \mathbf{A}_a : \mathbf{E} > \mathbf{0} \end{cases} \tag{11}$$

where $\mathbf{E}$ is the strain tensor, $\mathbf{A}_a = \mathbf{a}_a \otimes \mathbf{a}_a$ the texture tensor corresponding to each of the three preferred material directions defined by unit vector $\mathbf{a}_a$ ($\mathbf{a}_a \bullet \mathbf{a}_a = 1$, no sum over a), and the term $[\mathbf{A}_a : \mathbf{E}]$ represents the component of normal strain along the preferred direction of the unit vector $\mathbf{a}_a$.

Volumetric strain dependent aggregate modulus (H_{-A})

Experiments have shown that there a significant positive correlation between aggrecan content and compressive stiffness of the cartilage [30; 49]. It is assumed that the aggregate modulus of cartilage, H_{-A} is dependent on the change of aggrecan volume fraction ($\Delta\phi_G$) induced by the strain during cyclic loading. That is,

$$H_{-A} = a_1 \times \phi_G + a_2 \times \phi_G^2 \tag{12a}$$

where $\phi_G = \phi_{G0} + \Delta\phi_G$ (12b)

Here ϕ_{G0} is the initial aggrecan volume fraction when cartilage is under no external loading It is noted that 1% ϕ_G is the approximately the same as an aggrecan concentration of 18.4 mg of aggrecan/ml of cartilage tissue[4]. a_1 (MPa) and a_2 (MPa) are empirical constants to be fitted, but are required to be consistent with the study on human cartilage by Treppo et al. (2000) [49]. $\Delta\phi_G$ is the change of aggrecan volume fraction due to volumetric strain, $\varepsilon_V = J^s - 1$, which can be expressed as

$$\Delta\phi_G = \phi_{G0} \times \left(\frac{1}{1+\varepsilon_V} - 1 \right) = \phi_{G0} \times \left(\frac{1}{J^s} - 1 \right) \tag{13}$$

Using Equation (12), the aggregate modulus of cartilage can be expressed as

$$H_{-A} = H_{-A0} + \Delta H_{-A} \tag{14a}$$

where

$$\Delta H_{-A} = \left(a_1 + 2a_2\phi_{G0}\right)\Delta\phi_G + a_2\left(\Delta\phi_G\right)^2 \tag{14b}$$

Substituting Equations (12a-b), (13) and (14b) into (14a) leads to

$$H_{-A} = H_{-A0} + \left[a_1\phi_{G0} + a_2\phi_{G0}^2 \times \left(\frac{1}{J^s} + 1\right)\right]\left(\frac{1}{J^s} - 1\right) \tag{15}$$

Aggrecan content dependent hydraulic permeability

It is known that there is an inverse relation exists between cartilage aggrecan content and the hydraulic permeability of cartilage [29; 51]. Strains are induced in the cartilage tissue by surface loading, and it is necessary to modify the cartilage hydraulic permeability as a result of the change of aggrecan volume fraction ($\Delta\phi_G$) (Equation 12b). Consistent with the use of aggrecan concentration as a key factor contributing to the material properties of cartilage, we also use the aggrecan concentration to change the permeability of the cartilage tissue. To do this, we use the experimentally observed linear relationship on a log-log plot between cartilage permeability and glycoaminglycan volume fraction found by Zamparo and Comper (1989) [51],

$$\kappa = \frac{n\left(\phi_G\right)^m}{\mu} \tag{16}$$

where κ (m^4/Ns) is cartilage hydraulic permeability, μ (Ns/m^2) is water viscosity at 37ºC. *n* (m^2) and dimensionless *m* are parameters that determine the line equation on a log-log plot for the relationship between κ and ϕ_G. Note that for simplicity, we have taken the aggrecan concentration to be the equal to the glycosaminoglycan concentration. It is mentioned here in

passing that *m* is a negative dimensionless parameter, which indicates that permeability decreases with increasing ϕ_G.

Boundary conditions

As shown in Figure 1, the cylindrical cartilage specimen is loaded by a flat ended impervious indenter, and so it is reasonable to assume that there is no flux under loading in the *z*-direction but fluid can move in the *r*-direction (*i.e.* no boundary flux in the interval $0 \le r \le a$ at z = *0*). Outside the region of contact between the indentor and cartilage surface, a zero pressure boundary condition is assumed,

Outside the region of contact: $p(t) = 0$ when $a < r \le r_0$ at z=0 or $r = r_0$ (17a)

Inside the region of contact: $v^f(z = 0, t) = 0$ when $0 \le r \le a$ at z = 0 (17b)

At the bottom of cartilage (*i.e.* z = *h*), it is assumed that there is no fluid flow between cartilage and substrate bone, and displacements are fixed when z = *h*,

$$u_r^s(h,t) = 0;\ u_z^s(h,t) = 0 \tag{18}$$

At the outer edge of cartilage (*i.e.* $r = r_0$),

$$p(r_0, t) = 0 \tag{19}$$

Initial conditions

At *t = 0*, the equilibrium displacement of the cartilage solid matrix, the interstitial fluid pressure and velocity are set to zero throughout the cartilage tissue. The depth dependent initial equilibrium concentration is obtained as part of the calibration process in Section 3.

Numerical methods

The numerical solutions to the problem were obtained using the poroelastic model in the commercial Finite Element package COMSOL MULTIPHYSICS, which solves for the mechanical quantities (e.g. time dependent interstitial fluid and deformation of the solid matrix) in a material coordinate system [10]. The applied cyclic load was discretized into time steps. At each time step, the displacement of solid phase, the interstitial fluid pressure and fluid velocity were determined. A two-dimensional axisymmetric domain used 500 triangular elements with quadratic interpolation functions for all calculations, with a relative tolerance set to 10^{-3}. The FEM discretization of the time-dependent PDE was solved using an implicit solver of COMSOL MULTIPHYSICS[10]. The material parameters used in the model are shown in Table 1 and Table 2, which are typical for human knee cartilage[3; 5; 35].

RESULTS AND DISCUSSION

The experiments of Barker et al. (2001)[3] explored the deformation response of osteochondral plugs under a cyclic loading, with the cyclic load timing and magnitude set to approximate physiological loads experienced during walk-cycles in human adults. In Barker et al.'s (2000) experiments, cartilage specimens were obtained from human cadaveric knee joints. Osteochondral plugs were placed into Hanks' balanced salt solution and subjected to cyclic loading using a plane-end impervious indenter (3 mm in diameter). The applied cyclic loading cycle was chosen to approximate typical walking cycles as shown in Figure 1, *i.e.* the duration of a cycle = 1s, the load rise time = 20ms, the peak stress = 1.4 MPa, the duration of loading phase = 330 ms and the duration of recovery phase = 670 ms. Load and displacement measurements were performed during loading and recovery phases, respectively, for each load cycle.

Our aim is to now identify a set of poroelastic model parameters that describes the experimentally observed time-dependent deformation response of cartilage under cyclic

loading. To do this we need to fit an initial aggrecan volume fraction, the values for parameters a_1 and a_2 in Equation (12), while requiring the fitted values to be consistent with the data observed in the experimental study of Treppo et al (2002)[49]. Treppo et al (2002) reports measured strain-dependent aggregate modulus of cartilage in compression. We also need to fit the values for parameters *n* and *m* in Equation (16), while requiring them to be consistent with the data observed in the study of Zamparo and Comper (1989). The values of other parameters used in this study were fixed, as shown in Table 1 and Table 2.

Figure 2 compares our optimized model results with the experimental data from specimens labelled A_LPS (Figure 2a) and C_LFC (Figure 2b) in the Barker and Seedhom (2002). For specimen A_LPS, parameter values used in the model predictions were taken to be a_1 = 0.25 MPa, a_2 = 0.0155 MPa, n = 6.77 x 10^{-22} m^2, m = -2.37, initial aggrecan volume fraction $\phi_{G0}(z=0)$ = 2.7% and $\phi_{G0}(z=h)$ = 4%, whereas for specimen C_LFC, initial aggrecan volume fraction was found to be $\phi_{G0}(z=0)$ = 2.2% and $\phi_{G0}(z=h)$ = 3.2 %, and n = 4.17x 10^{-22} m^2 with no change of other parameters.

The selected initial aggrecan concentration falls within the range of measured aggrecan concentration in cartilage [49]. Further, the initial value of hydraulic permeability κ is consistent with the findings of previous experimental studies (*i.e.*, 1-5 x 10^{-15} m^4/Ns)[32; 35]. It can be seen that numerical results with volumetric strain dependent aggregate modulus and permeability can fit experimentally measured exudation and total strains very well.

As shown in Figure 2c, there are two deformation processes with different time scales. The first is the consolidation of the cartilage (a relatively slow process), while the second process is the strain of the cartilage due to an individual load cycle (a relatively fast process). The cyclic strains form an ‘envelope’ as the consolidation process evolves. We refer to the

top of the envelope as the ‘exudation strain’, while the bottom of the envelope is referred to here as the ‘total strain’ (see Figure 2c).

Importantly, if instead of our model presented above we assumed a constant aggregate modulus (H_0), we find that the model can only capture the measured deformation behaviour of cartilage at initial loading (*i.e.* first 400s), but not the later times. A constant aggregate modulus may result in significant overestimation of both exudation and total strains with the increase of loading time. This highlights the importance of using a strain dependent aggregate modulus.

In our model the parameters a_1 and a_2 govern the influence changes in the aggrecan content during deformation has on the compressive stiffness of cartilage ECM, refer to Equation (12). The effects of the variation these two model parameters have on both total and exudation strains are shown in Figure 3. A two-fold increase of a_1 shifts both exudation strain and total strain curves up (i.e. towards smaller strains), while simultaneously closing the distance between these two curves. On the other hand, although a two-fold increase of a_2 shifts both exudation strain and total strain curves up, there is little change in the distance between these two curves. This difference in the relative effects that the parameters a_1 and a_2 have on the load deformation cyclic loading envelope shows they contain different information about the non-linear stiffness response of the cartilage tissue. Importantly, the two degrees of freedom permitted by the parameters a_1 and a_2 enables our constitutive model to be adjusted to closely match both exudation and total strain curves observed in the experiments.

As shown in Equations (12) – (15), the mechanical properties of cartilage in compression is determined by the aggrecan concentration within the tissue. We note that the aggrecan content of articular cartilage varies between different joints and at different sites

within joints, but this model is capable of capturing the tissue response to variations of initial aggrecan content between joints and within joints.

Under external loading, the change of volumetric strain results in the variation of aggrecan concentration which modifies the aggregate modulus, and ultimately the deformation response of cartilage. Figure 4 shows the volumetric strain at four different depths from the cartilage surface to the deep zone. It can be seen that the volumetric strain significantly increases from the deep zone to the superficial zone (the magnitude of the volume strain in the superficial zone is more than three-fold higher than it is in deep zone). In addition, the volumetric strain changes rapidly during the first 500 cycles (duration of each cycle is 1s), as the fluid is squeezed out of the tissue during this initial loading stage.

For the cartilage tissue to survive the challenging external mechanical conditions, cartilage homeostatic responses are tuned to adjust matrix biosynthesis and ECM turnover. The properties of the ECM reach a steady state based on intra-tissue chemical and mechanical stimuli detected by the chondrocytes. Important signals detected by chondrocytes centre on the local aggrecan concentration, the local strain profile and the local hydrostatic pressure distribution. Note various studies postulated that articular cartilage superficial and upper transitional zone represents an important signalling centre that is involved in regulation of tissue homeostasis [13; 33],. Our findings suggest that the superficial and upper transitional zones may be vulnerable to injury arising from excessive deformation (*e.g.* during traumatic joint injury) which may lead to the development of OA [25].

Figure 5 shows the depth dependent percent increase in the maximum: (a) aggrecan volume fraction, (b) aggregate modulus (H_{-A}), and (c) interstitial fluid pressure for different numbers of loading cycles (Specimen A_LPS). The time-dependent percent change is calculated by using the maximum aggrecan volume fraction, aggregate modulus and

interstitial fluid pressure in first loading cycle as the reference state. As shown in Figure 5a, for the long time scales, the volumetric strain during cyclic loading corresponds to around a 200% increase of aggrecan concentration in the superficial zone and around a 60% increase in the deep zone. In turn these changes in aggrecan concentration correspond to around 100% increase of H_{-A} near the cartilage surface and 25% in the deep zone (Figure 5b). In addition, as shown in Figure 5c, the steady-state interstitial fluid pressure will decrease 60% near the cartilage surface and 40% in the deep zone compared to that at initial stage of loading, which means significant amount of load will be transferred to the ECM at steady-state.

In vivo studies of the cartilage deformation response to dynamic exercise show that cartilage takes time to recover it initial shape following loading [14]. In this study, we conducted a series of numerical experiments to understand the deformation recovery behaviour of the cartilage osteochondral plugs after different numbers of loading cycles. It can be seen from Figure 6 that the absolute time for recovery is very similar once the exudation deformation approaches a large proportion of its steady-state value (i.e. 2170s vs 500 cycles; 2360 vs 1000 cycles; 2460 vs 2000 cycles; 2470 vs 3000 cycles). The results suggest that after reaching steady-state deformation under the laboratory test conditions, the osteochondral plugs require around 40 mins to fully recover after the loading is removed. We note that an *in vivo* study by Eckstein et al (1999) revealed that a period of 90 mins was required for patellar cartilage to fully recover its initial profile after 100 knee bends[14].

Over short time scales, the amount of fluid that is squeezed out of the tissue during the loading phase within a loading cycle is greater than that being imbibed during the unloaded phase of the cycle. Consequently, this imbalance leads to a significant increase in tissue deformation over time. The loss of fluid implies that some portion of deformation at the cartilage surface is not fully recovered during a loading cycle, which results in what we refer to as ‘exudation strain’. At long time scales, the amount of fluid squeezed out with each load

cycle is exactly equal to the amount imbibed during unloading cycle, and so both total and exudation strains gradually reach an equilibrium with this steady state fluid oscillation.

Numerous studies have reported the effects of strain dependent permeability on cartilage deformation over the last decade[21; 27; 34; 39; 41]. It has been observed that cartilage permeability strongly depends on deformation, with a reduction of approximately 50% in permeability for a 10% volumetric compression. It is also known that hydraulic permeability increases significantly with age[42], and this increase could affect the time dependent deformation behaviour of cartilage under external loading. Figure 7 investigates the effects of the magnitude of initial permeability (κ_0) (which is estimated from the initial aggrecan volume fraction using Equation (16)), on the exudation and total strain respectively. A higher permeability is seen to significantly reduce the time for the tissue deformation to reach its steady-state by allowing interstitial fluid to more rapidly flow out of the tissue under external loading.

The model was then used to predict the deformation response of cartilage under various loading conditions. As shown in Figure 8, by fixing the loading duration of a loading cycle (i.e. 1s), the effects of the loading-to-recovery ratio (t_l / t_R) on time dependent total and exudation strains are explored. The load-deformation response of the tissue under cyclic loading is also compared to that for a constant loading with a magnitude of P_{max} (1.4MPa). It can be seen that for an increasing loading-to-recovery ratio, the total strain gradually approaches that for the constant loading. This shows that there is a significant variation in deformation response of cartilage with the fraction of time spent loaded during in each load cycle..

Our previous studies [15; 54; 56] have demonstrated that the interstitial fluid flow induced by cyclic loading enhances the transport of solutes (*e.g.* IGF-I) into cartilage, and that a

combination of higher loading frequencies (*e.g.*, 1 Hz) and high strain amplitude (*e.g.*, 10%) results in the greatest transport enhancement. We also note that as both experimental and theoretical studies have also shown a strong correlation between interstitial fluid flow, transport and chondrocyte mediated ECM biosynthesis [7; 55; 57; 59], the current model will enable more accurate prediction of cartilage homeostasis on account of having more realistic information about the deformation and interstitial fluid velocities within the tissue.

A summary of the main results are as follows:

- The depth dependent deformation, stiffness and permeability responses of human cartilage upon commencement and cessation of cyclic loading have been quantitated in detail for a particular explant experimental system.
- It has been shown that the load-deformation response of human cartilage tissue can be accurately represented using a biphasic non-linear poroelastic model with volumetric strain dependent aggregate modulus and permeability. Experimentally measured exudation and total strains on human cartilage explants can be fitted very well using a minimal set of model parameters that are consistent with the published literature.
- The volumetric strain is largest in the superficial zone and decreases with depth, being least in the deep zone. The volumetric strain changes rapidly during the initial stage of loading as net fluid is squeezed out during consolidation of the tissue.
- A higher permeability significantly reduces the time for the tissue deformation to reach its steady-state by allowing interstitial fluid to more rapidly exit the tissue under external loading.
- There is a significant variation in deformation response of cartilage under cyclic loading depending on the loading-to-recovery ratio within a load cycle.

ACKNOWLEDGEMENTS

The authors wish to thank the National Health and Medical Research Council, Australian Government (grant Ref APP1051538) and NIH Grant AR060331 for support.

REFERENCES

1. Ateshian GA, NO Chahine, IM Basalo, CT Hung. The correspondence between equilibrium biphasic and triphasic material properties in mixture models of articular cartilage. Journal of Biomechanics 37: 391–400, 2004.

2. Bachrach NM, WB Valhmu, E Stazzone, A Ratcliffe, WM Lai, VC Mow. Changes in Proteoglycan Synthesis of Chondrocytes In Articular Cartilage Are Associated With The Time-Dependent Changes In Their Mechanical Environment. Journal of Biomechanics 28: 1561-1569, 1995.

3. Barker MK, BB Seedhom. The relationship of the compressive modulus of articular cartilage with its deformation response to cyclic loading: does cartilage optimize its modulus so as to minimize the strains arising in it due to the prevalent loading regime? . Rheumatology 40: 274-284, 2001.

4. Basser PJ, R Schneiderman, RA Bank, E Wachtel, A Maroudas. Mechanical properties of the collagen network in human articular cartilage as measured by osmotic stress technique. Archives of Biochemistry and Biophysics 351: 207-219, 1998.

5. Bonassar LJ, AJ Grodzinsky, A Srinivasan, SG Davila, SB Trippel. Mechanical and physiochemical regulation of the action of insulin-like growth factor-i on articular cartilage. Archives of Biochemistry and Biophysics 379: 57-63, 2000.

6. Burasc PM, TW Obitz, SR Eisenberg, D Stamenovic. Confined and unconfined stress relaxation of cartilage: appropriateness of a transversely isotropic analysis. Journal of Biomechanics 32: 1125-1130, 1999.

7. Buschmann MD, YA Gluzband, AJ Grodzinsky, EB Hunziker. Mechanical compression modulates matrix biosynthesis in chondrocyte/agarose culture. Journal of Cell Science 108: 1497-1508, 1995.

8. Buschmann MD, Y-J Kim, M Wong, E Frank, EB Hunziker, AJ rodzinsky. Stimulation of aggrecan synthesis in cartilage explants by cyclic loading is localized to regions of high interstitial fluid flow. Archives of Biochemistry and Biophysics 366: 1-7, 1999.

9. Chahine NO, FH Chen, CT Hung, GA Ateshian. Direct Measurement of Osmotic Pressure of Glycosaminoglycan Solutions by Membrane Osmometry at Room Temperature. Biophysical Journal 89: 1543–1550, 2005.

10. COMSOL-Multiphysics. MA, USA: COMSOL, Inc: 2012.

11. Curnier A, Q-C He, P Zysset. Conewise linear elastic materials. Journal of Elasticity 37: 1-38, 1995.

12. Disilvestro MR, J-KF Suh. Biphasic Poroviscoelastic Characteristics of Proteoglycan-Depleted Articular Cartilage: Simulation of Degeneration. Annals of Biomedical Engineering 30: 2002.

13. Dowthwaite GP, JC Bishop, SN Redman, IM Khan, P Rooney, DJR Evans, L Haughton, Z Bayram, S Boyer, B Thomson, MS Wolfe, CW Archer. The surface of articular cartilage contains a progenitor cell population. Journal of Cell Science 117: 889-897, 2004.

14. Eckstein F, M Tieschky, S Faber. Functional analysis of articular cartilage deformation, recovery,and fluid flow following dynamic exercise in vivo. Anat Embryol 200: 419-424, 1999.

15. Gardiner BS, DW Smith, P Pivonka, AJ Grodzinsky, EH Frank, L Zhang. Solute transport in cartilage undergoing cyclic deformation. Computer Methods in Biomechanics and Biomedical Engineering 10: 265-278, 2007.

16. Gardiner BS, L Zhang, DW Smith, P Pivonka, AJ Grodzinsky. A mathematical model for targeting chemicals to tissues by exploiting complex degradation. Biology Direct 6: 1-16, 2011.

17. Gray ML, AM Pizzanelli, AJ Grodzinsky, RC Lee. Mechanical and physicochemical determinants of the chondrocyte biosynthetic response. Journal of Orthopaedic Research 6: 777-792, 1988.

18. Grodzinsky AJ, ME Levenston, M Jin, EH Frank. Cartilage tissue remodeling in response to mechanical forces. Annual Review of Biomedical Engineering 2: 691-713, 2000.

19. Guilak F, VC Mow. The mechanical environment of the chondrocyte: a biphasic finite element model of cell-matrix interactions in articular cartilage. Journal of Biomechanics 33: 1663-1673, 2000.

20. Heinegård D, A Oldberg. Structure and biology of cartilage and bone matrix noncollagenous macromolecules. The FASEB Journal 3: 2042-2051, 1989.

21. Holmes MH, VC Mow. The Nonlinear Characteristics of Soft Gels And Hydrated Connective Tissues In Ultrafiltration. J Biomechanics 23: 1145-1156, 1990.

22. Kestin J, M Sokolov, WA Wakeham. Viscosity of liquid water in the range −8 °C to 150 °C. Journal of Physicaland Chemical Reference Data 7: 941-948, 1978.

23. Kiani C, L Chen, YJ Wu, AJ Yee, BB Yang. Structure and function of aggrecan. Cell Res 12: 19-32, 2002.

24. Krishnan R, FE Seonghun Park, GA Ateshian. Inhomogeneous cartilage properties enhance superficial interstital fluid support and frictional properties, but do not provide a homogenous state of stress. Journal of Biomechanical Engineering 125: 569-577, 2003.

25. Kurz B, AK Lemke, J Fay, T Pufe, AJ Grodzinsky, M Schünke. Pathomechanisms of cartilage destruction by mechanical injury. Annals of Anatomy 187: 473-485, 2005.

26. Lai WM, JS Hou, VC Mow. A triphasic theory for the swelling and deformation behaviors of articular cartilage. journal of Biomechanical Engineering 113: 245-258, 1991.

27. Lai WM, VC Mow, V Roth. Effects of nonlinear strain-dependent permeability and rate of compression on the stress behavior of articular cartilage. Journal of Biomechanical Engineering 103: 61-66, 1981.

28. Lee DW, X Banquy, JN Israelachvili. Stick-slip friction and wear of articular joints. Proc Natl Acad Sci U S A 110: E567–E574, 2013.

29. Loret B, FMF Simões. Articular cartilage with intra- and extrafibrillar waters: a chemo-mechanical model. Mechanics of Materials 36: 515-541, 2004.

30. Lu XL, DDN Sun, XE Guo, FH Chen, WM Lai, VC Mow. Indentation determined mechanoelectrochemical properties and fixed charge density of articular cartilage Annals of Biomedical Engineering 32: 370-379, 2004.

31. Maroudas A. Physicochemical properties of articular cartilage. In: Adult Articular Cartilage, edited by M A R Freeman Kent, UK: Pitman Medical: 215–290, 1979.

32. Mauck RL, CT Hung, GA Ateshian. Modeling of neutral solute transport in a dynamically loaded porous permeable gel: implications for articular cartilage biosynthesis and tissue engineering. Journal of Biomechanical Engineering 125: 602-614, 2000.

33. Mow VC, WC Hayes. Basic orthopaedic biomechanics (2nd edition). Lippincoot - Raven Publishers, Philadephia: 1997.

34. Mow VC, MH Holmes, WM Lai. Fluid transport and mechanical properties of articular cartilage: a review. Journal of Biomechanics 17: 377-394, 1984.

35. Mow VC, JS Hou, JM Owens, A Ratcliffe. Biphasic and quasilinear viscoelastic theories for hydrated soft tissues. Biomechanics of Diarthrodial Joints, Springer-Verlag, New York: 215-260, 1990.

36. Muir H. Proteoglycan of cartilage. Journal of Clinical Pathology 12: 67-81, 1978.

37. Oloyede A, ND Broom. The generalized consolidation of articular cartilage: an investigation of its near-physiological response to static load. Connective Tissue Research 31: 75-86, 1994.

38. Oloyede A, ND Broom. Is classical consolidation theory applicable to articular cartilage deformation? Clinical Biomechanics 6: 206-212, 1991.

39. Quinn TM, P Dierickx, AJ Grodzinsky. Glycosaminoglycan network geometry may contribute to anisotropic hydraulic permeability in cartilage under compression. Journal of Biomechanics 34: 1483–1490, 2001.

40. Quinn TM, AJ Grodzinsky, MD Buschmann, Y-J Kim, EB Hunziker. Mechanical compression alters proteoglycan deposition and matrix deformation around individual cells in cartilage explants. Journal of Cell Science 111: 573-583, 1998.

41. Reynaud B, TM Quinn. Anisotropic hydraulic permeability in compressed articular cartilage. Journal of Biomechanics 39: 131–137, 2006.

42. Rotter N, G Tobias, M Lebl, AK Roy, MC Hansen, CA Vacanti, LJ Bonassar. Age-related changes in the composition and mechanical properties of human nasal cartilage. Archives of Biochemistry and Biophysics 403: 132-140, 2002.

43. Sah RL-Y, Y-J Kim, J-YH Doong, AJ Grodzinsky, AHK Plass, JD Sandy. Biosynthetic response of cartilage explants to dynamic compression. Journal of Orthopaedic Research 7: 619-636, 1989.

44. Setton LA, DM Elliott, VC Mow. Altered mechanics of cartilage with osteoarthritis: human osteoarthritis and an experimental model of joint degeneration Osteoarthritis and Cartilage 7: 2-14, 1999.

45. Smith DW, BS Gardiner, JB Davidson, AJ Grodzinsky. Computational model for the analysis of cartilage and cartilage tissue constructs. Tissue Engineering and Regenerative Medicine DOI: 10.1002/term.1751: 2013.

46. Soltz MA, GA Ateshian. A conewise linear elasticity mixture model for the analysis of tension-compression nonlinearity in articular cartilage. Journal of Biomechanical Engineering 122: 576-586, 2000.

47. Spilker RL, J-K Suh. Formulation and evaluation of a finite element model for the biphasic model of hydrated soft tissues. Computers and Structures 35: 425-439, 1990.

48. Sun DN, WY Gu, XE Guo, WM Lai, VC Mow. A mixed finite element formulation of triphasic mechano-electrochemical theory for charged, hydrated biological soft tissues. International Journal For Numerical Methods In Engineering 45: 1375-1402, 1999.

49. Treppo S, H Koepp, EC Quan, AA Cole, KE Kuettner, AJ Grodzinsky. Comparison of biomechanical and biochemical properties of cartilage from human knee and ankle pairs. Journal of Orthopaedic Research 18: 739–748, 2000.

50. Wu JZ, W Herzog. Elastic anisotropy of articular cartilage is associated with the microstructures of collagen fibers and chondrocytes. Journal of biomechanics 35: 931-942, 2002.

51. Zamparo O, WD Comper. Hydraulic conductivity of chondroitin sulfate proteoglycan solutions. Archives of Biochemistry and Biophysics 274: 259-269, 1989.

52. Zhang L. Solute transport in cyclic deformed heterogeneous articular cartilage. International Journal of Applied Mechanics 3: 1-18, 2011.

53. Zhang L. Solute transport in cyclic deformed heterogeneous articular cartilage. International Journal of Applied Mechanics 3: 507-524, 2011.

54. Zhang L, BS Gardiner, DW Smith, P Pivonka, AJ Grodzinsky. The effect of cyclic deformation and solute binding on solute transport in cartilage. Archives of Biochemistry and Biophysics 457: 47-56, 2007.

55. Zhang L, BS Gardiner, DW Smith, P Pivonka, AJ Grodzinsky. A fully coupled poroelastic reactive-transport model of cartilage. Molecular & Cellular Biomechanics 5: 133-153, 2008.

56. Zhang L, BS Gardiner, DW Smith, P Pivonka, AJ Grodzinsky. IGF uptake with competitive binding in articular cartilage. Journal of Biological Systems 16: 175-195, 2008.

57. Zhang L, BS Gardiner, DW Smith, P Pivonka, AJ Grodzinsky. Integrated model of IGF-I mediated biosynthesis in deforming articular cartilage. Journal of Engineering Mechanics 135: 439-449, 2009.

58. Zhang L, BS Gardiner, DW Smith, P Pivonka, AJ Grodzinsky. Integrated model of IGF-I mediated biosynthesis in deforming articular cartilage. Journal of Engineering Mechanics (ASCE) 135: 439-449, 2009.

59. Zhang L, BS Gardiner, DW Smith, P Pivonka, AJ Grodzinsky. 2010. The Transport of Insulin-like Growth Factor through Cartilage. In: Vafai K editor. Porous Media: Applications in Biological Systems and Biotechnology: Taylor & Francis Group.

60. Zhang L, M Richardson, P Mendis. The role of chemical and mechanical stimuli in mediating bone fracture healing. Clinical and Experimental Pharmacology and Physiology In press, 2011.

Table caption

Table 1: Material parameters used for comparison with Barker et al.'s experimental data [3]

Table 2 Depth dependent cartilage material properties used in this study[24]

Figure caption

Figure 1 Schematic of deformation response of cartilage specimen under cyclic loading (a = 1.5 mm, r_0 = 12 mm, h_0 = 2.8 mm). Depiction of the cyclic loading applied in the model to simulate a walking gait cycle. The total duration of one loading cycle = t_L (0.33s) + t_R (0.67s) = 1s. The peak stress P_{max} = 1.4MPa.

Figure 2 Comparison of numerical predictions with experimental results Barker et al. (2001) [3]. The duration of one loading cycle = 1s. (a) Specimen A_LPS (2.8 mm thick): The parameters used in model prediction are a_1 = 0.25 MPa, a_2 = 0.0155 MPa, n = 6.77x 10^{-22} m^2, m = -2.37, initial aggrecan volume fraction $\phi_{G0}(z=0)$ = 2.7% and $\phi_{G0}(z=h)$ = 4%; (b) Specimen C_LFC (2.2 mm thick): The parameters used in model prediction are a_1 = 0.25, a_2 = 0.0155, n = 4.17 x 10^{-22} m^2, m = -2.37, initial aggrecan volume fraction $\phi_{G0}(z=0)$ = 2.2%

and $\phi_{G0}(z=h)$ = 3.2 %; (c) Time dependent exudation and total strain at cartilage surface (Specimen A_LPS) during the first 50 loading cycles.

Figure 3 Parametric study of time-dependent total and exudation strains at cartilage surface (Specimen A_LPS). The duration of one loading cycle = 1s.

Figure 4 Depth dependent volumetric strain at loading phase at different loading cycles (Specimen A_LPS). The duration of one loading cycle = 1s.

Figure 5 Depth dependent percent increase in the maximum: (a) aggrecan volume fraction, (b) aggregate modulus (H_{-A}), and (c) interstitial fluid pressure, for different number of loading cycles (Specimen A_LPS). The time-dependent percent increase is calculated by using the maximum aggrecan volume fraction, aggregate modulus and interstitial fluid pressure in first loading cycle as the reference value. The duration of one loading cycle = 1s.

Figure 6 Time-dependent exudation strain profiles when applied cyclic loading is removed after different loading cycles (Specimen A_LPS). The duration of one loading cycle = 1s.

Figure 7 The effects of permeability on time dependent total and exudation strains respectively (Specimen A_LPS). κ_0 is initial cartilage permeability which depends on the initial aggrecan volume fraction. The duration of one loading cycle = 1s.

Figure 8 The effects of loading-to-recovery ratio (t_l / t_R) on time dependent total and exudation strains respectively. The magnitude of the constant load = P_{max} = 1.4MPa. The duration of one loading cycle = 1s and t_{l0} = 20ms (Specimen A_LPS).

Table 1: Material parameters used for comparison with Barker et al.'s experimental data [3]

Parameter	**Value**	**Ref**
Fluid phase volumetric fraction (ϕ^f)	0.8	[5; 35]
Load rise time (t_{L0})	0.02s	[3]
Loading phase duration (t_L)	0.33s	[3]
Recovery phase duration (t_R)	0.67s	[3]
Peak stress ($\sigma_{\max}$)	1.4 MPa	[3]
μ (water viscosity at 37ºC)	7 x 10^{-4} Ns/m^2	[22]

Table 2 Depth dependent cartilage material properties used in this study[24]

Location	Tensile modulus (MPa)		Shear modulus (MPa)
	Horizontal	Vertical	
Superficial zone	10	6	3
Middle zone	6	6	3
Deep zone	4	15	2

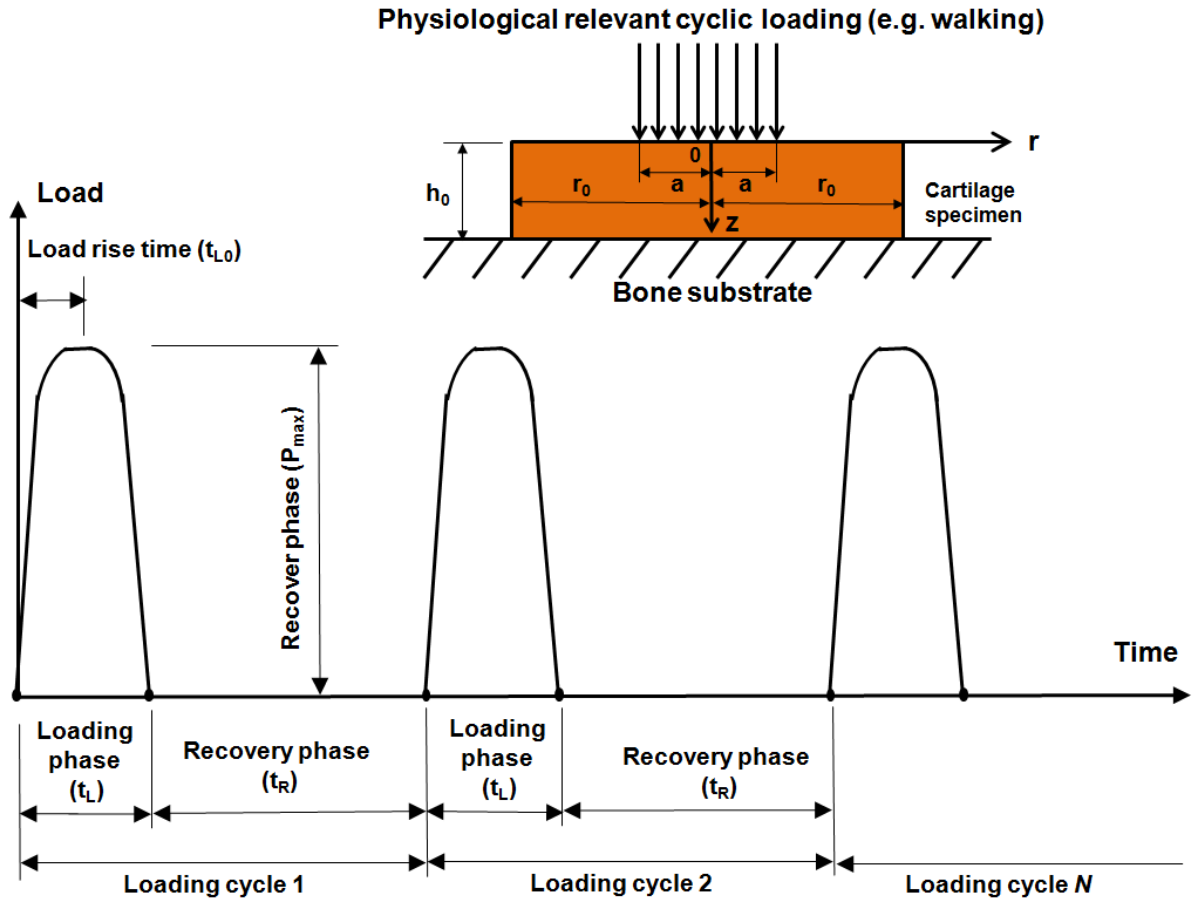

Figure 1 Schematic of deformation response of cartilage specimen under cyclic loading (a = 1.5 mm, r_0 = 12 mm, h_0 = 2.8 mm). Depiction of the cyclic loading applied in the model to simulate a walking gait cycle. The total duration of one loading cycle = t_L (0.33s) + t_R (0.67s) = 1s. The peak stress P_{max} = 1.4MPa.

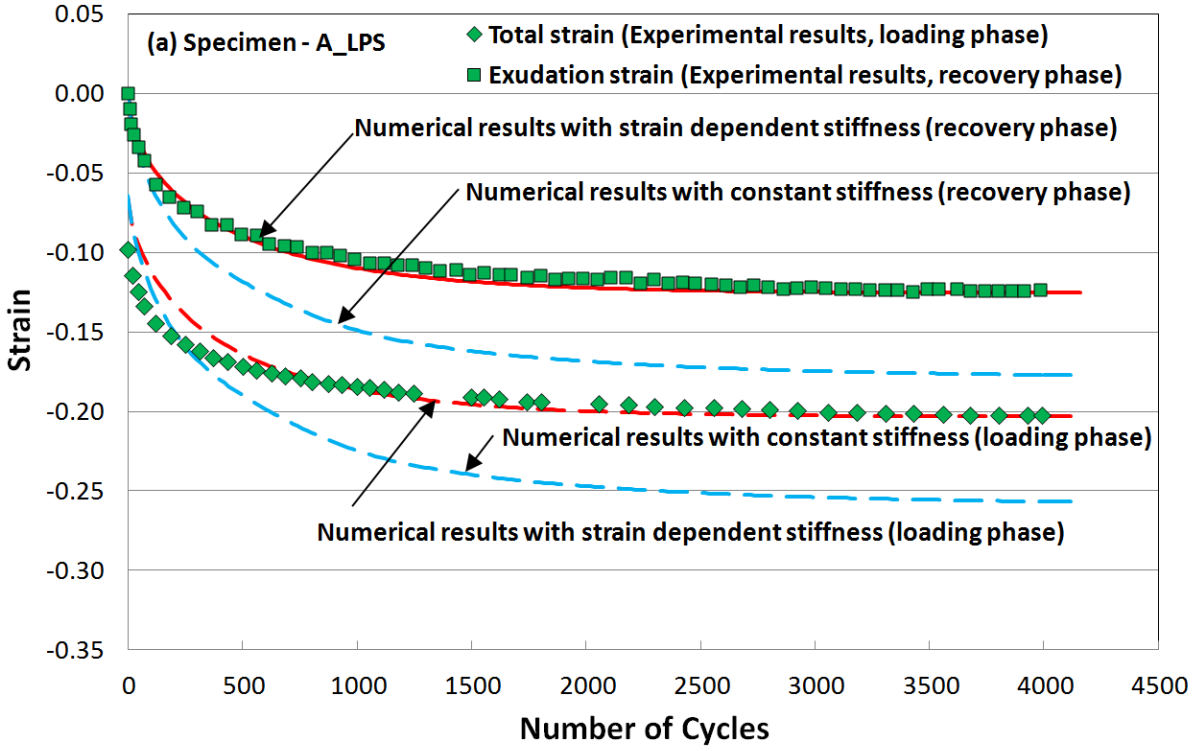
(a) Specimen - A_LPS
Total strain (Experimental results, loading phase)
Exudation strain (Experimental results, recovery phase)
Numerical results with strain dependent stiffness (recovery phase)
Numerical results with constant stiffness (recovery phase)
Numerical results with constant stiffness (loading phase)
Numerical results with strain dependent stiffness (loading phase)
Strain
Number of Cycles
0.05
0.00
-0.05
-0.10
-0.15
-0.20
-0.25
-0.30
-0.35
0
500
1000
1500
2000
2500
3000
3500
4000
4500

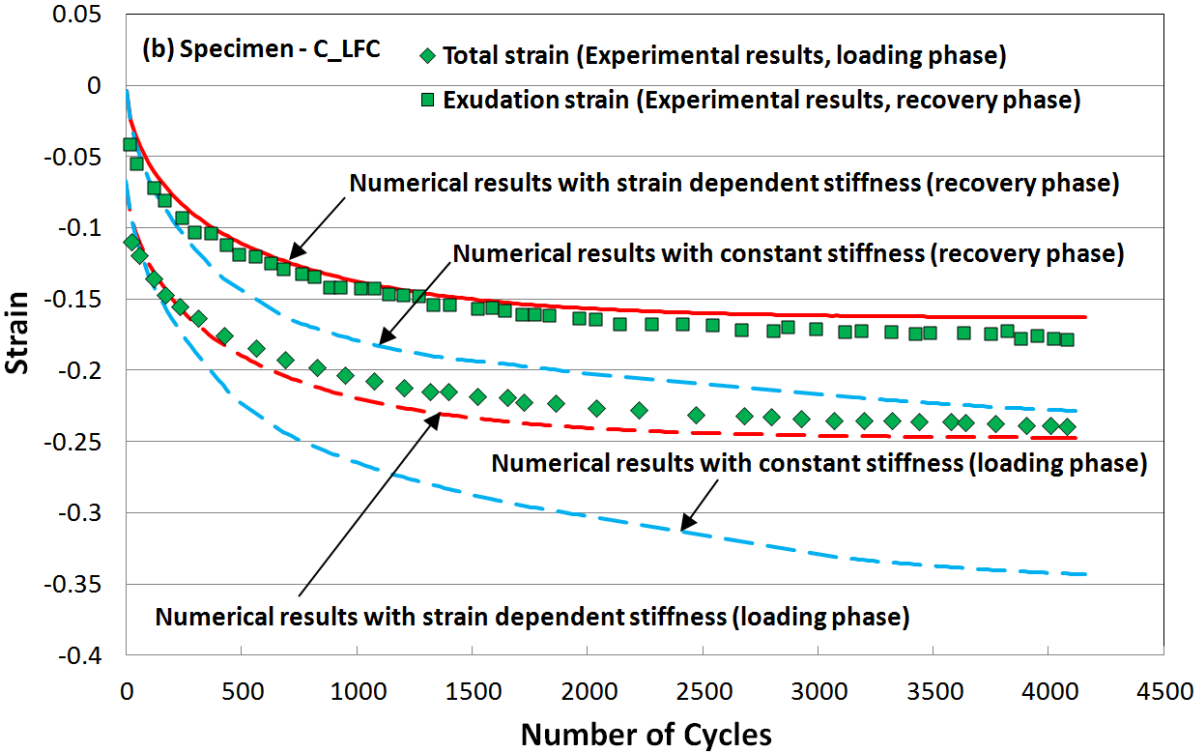
(b) Specimen - C_LFC
Total strain (Experimental results, loading phase)
Exudation strain (Experimental results, recovery phase)
Numerical results with strain dependent stiffness (recovery phase)
Numerical results with constant stiffness (recovery phase)
Numerical results with constant stiffness (loading phase)
Numerical results with strain dependent stiffness (loading phase)
Strain
Number of Cycles
0.05
0
-0.05
-0.1
-0.15
-0.2
-0.25
-0.3
-0.35
-0.4
0
500
1000
1500
2000
2500
3000
3500
4000
4500

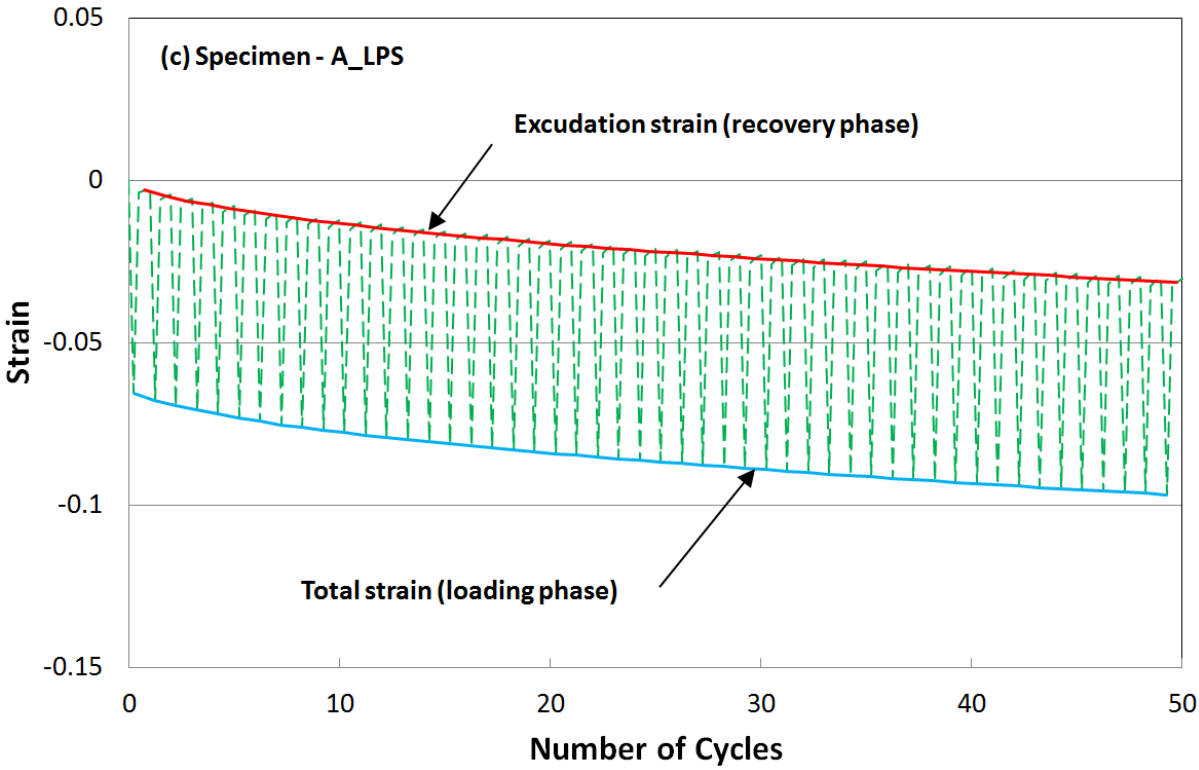

Figure 2 Comparison of numerical predictions with experimental results Barker et al. (2001) [3]. The duration of one loading cycle = 1s. (a) Specimen A_LPS (2.8 mm thick): The parameters used in model prediction are a_1 = 0.25 MPa, a_2 = 0.0155 MPa, n = 6.77x 10^{-22} m^2, m = -2.37, initial aggrecan volume fraction $\phi_{G0}(z=0)$ = 2.7% and $\phi_{G0}(z=h)$ = 4%; (b) Specimen C_LFC (2.2 mm thick): The parameters used in model prediction are a_1 = 0.25, a_2 = 0.0155, n = 4.17 x 10^{-22} m^2, m = -2.37, initial aggrecan volume fraction $\phi_{G0}(z=0)$ = 2.2% and $\phi_{G0}(z=h)$ = 3.2 %; (c) Time dependent exudation and total strain at cartilage surface (Specimen A_LPS) during the first 50 loading cycles.

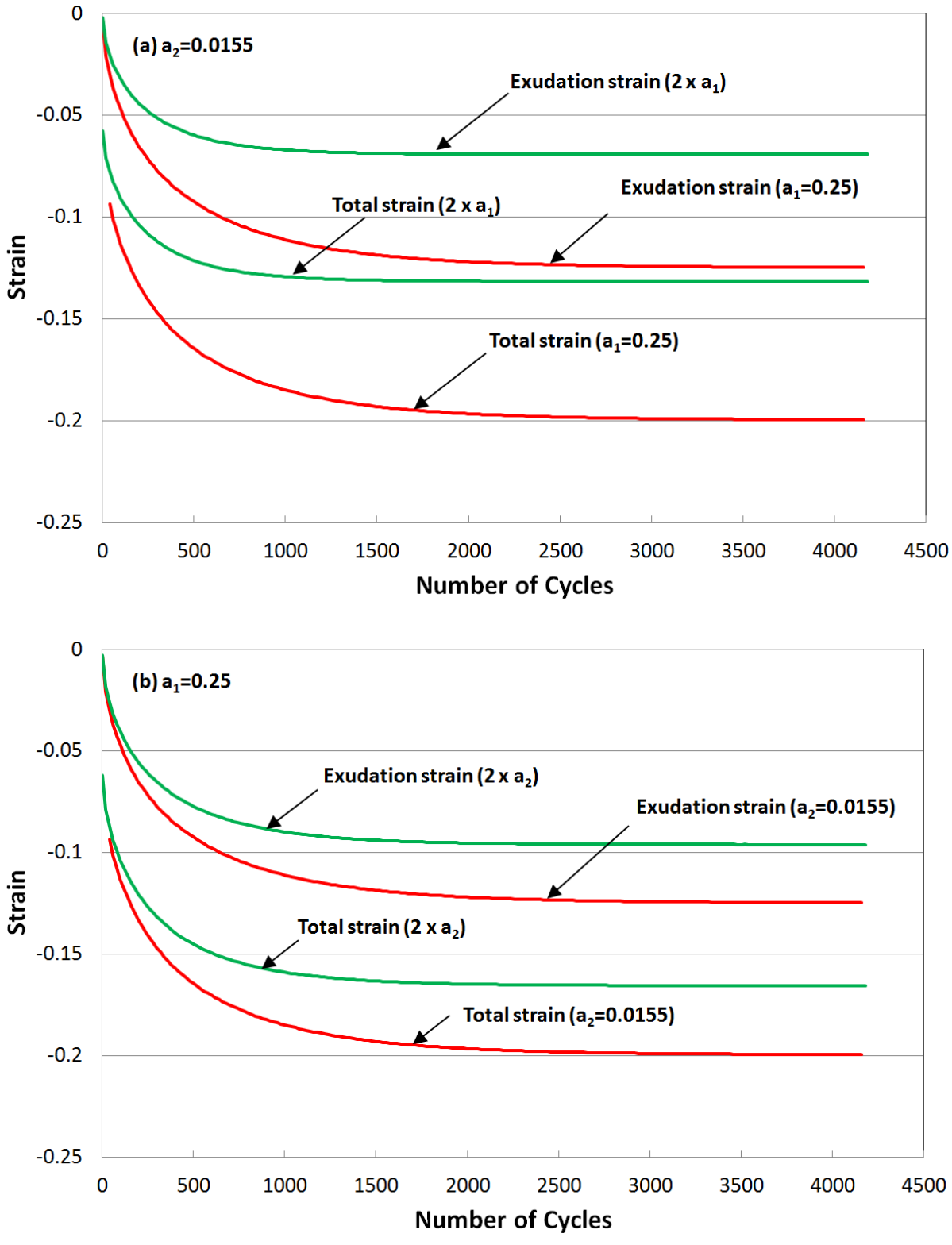

Figure 3 Parametric study of time-dependent total and exudation strains at cartilage surface (Specimen A_LPS). The duration of one loading cycle = 1s.

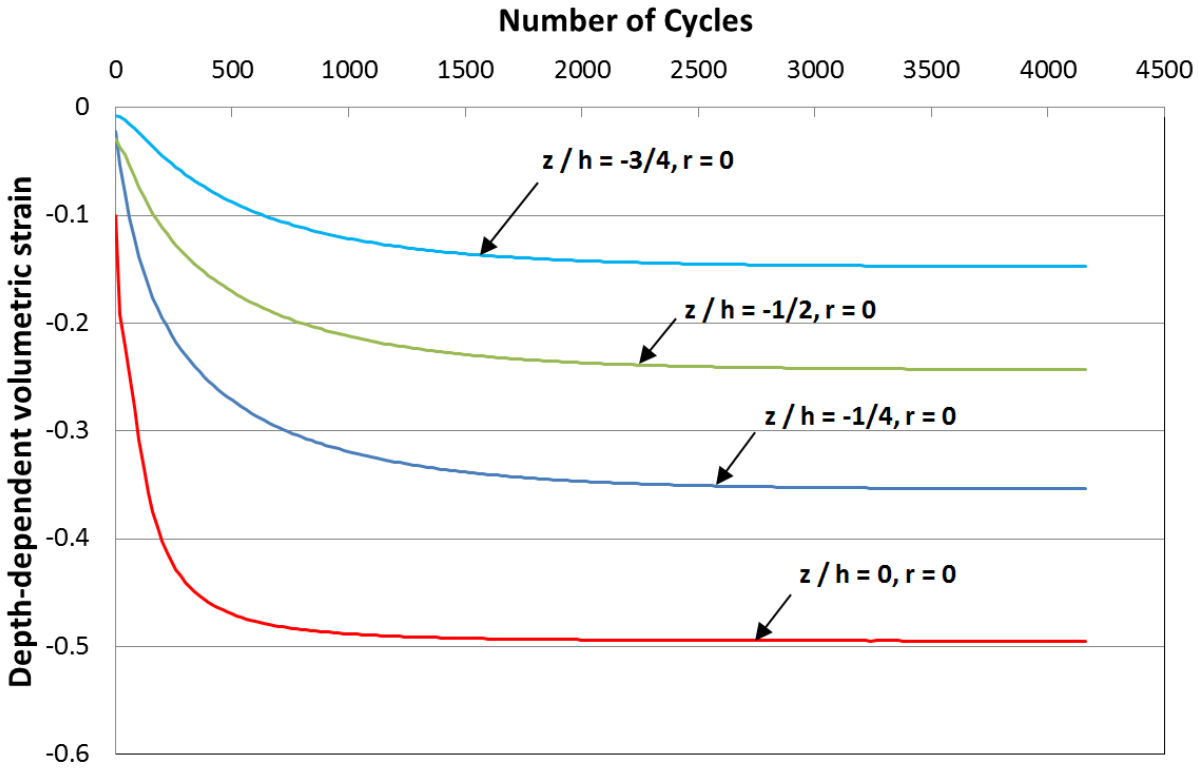

Figure 4 Depth dependent volumetric strain at loading phase at different loading cycles (Specimen A_LPS). The duration of one loading cycle = 1s.

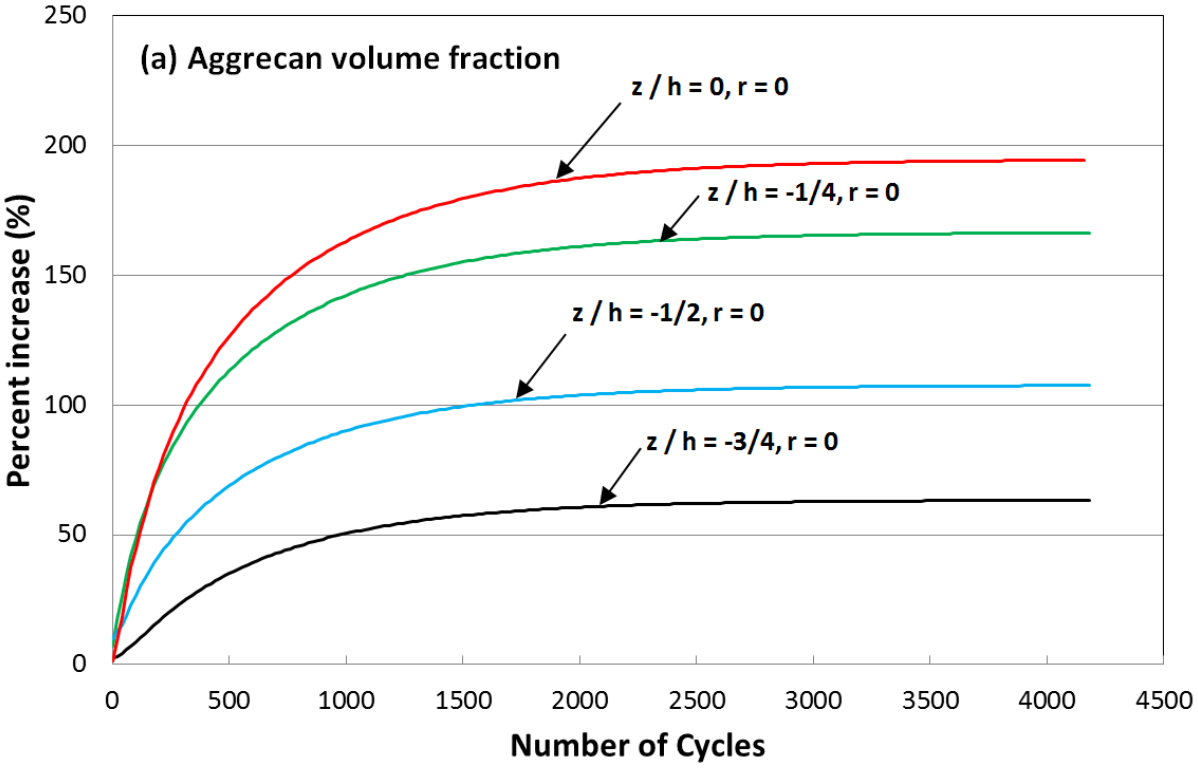
(a) Aggrecan volume fraction
z / h = 0, r = 0
z / h = -1/4, r = 0
z / h = -1/2, r = 0
z / h = -3/4, r = 0
Percent increase (%)
Number of Cycles
0
50
100
150
200
250
0
500
1000
1500
2000
2500
3000
3500
4000
4500

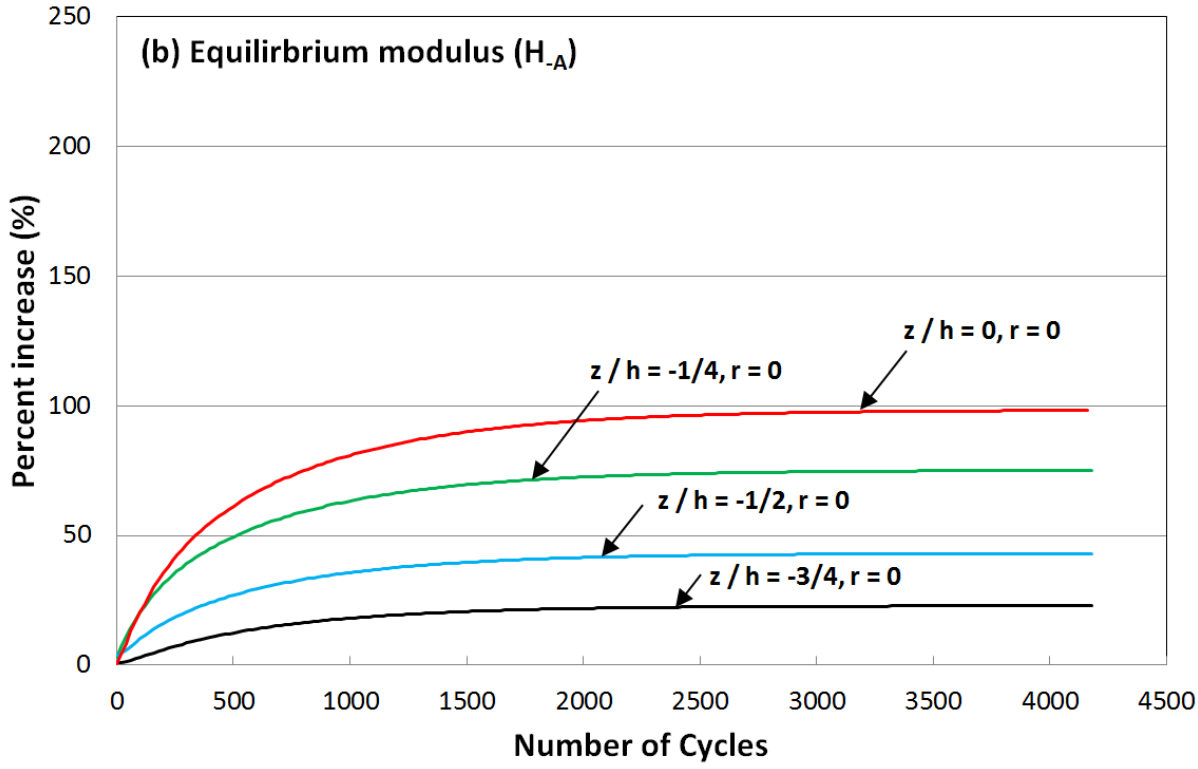
(b) Equilirbrium modulus (H-A)
z / h = 0, r = 0
z / h = -1/4, r = 0
z / h = -1/2, r = 0
z / h = -3/4, r = 0
Percent increase (%)
Number of Cycles
0
50
100
150
200
250
0
500
1000
1500
2000
2500
3000
3500
4000
4500

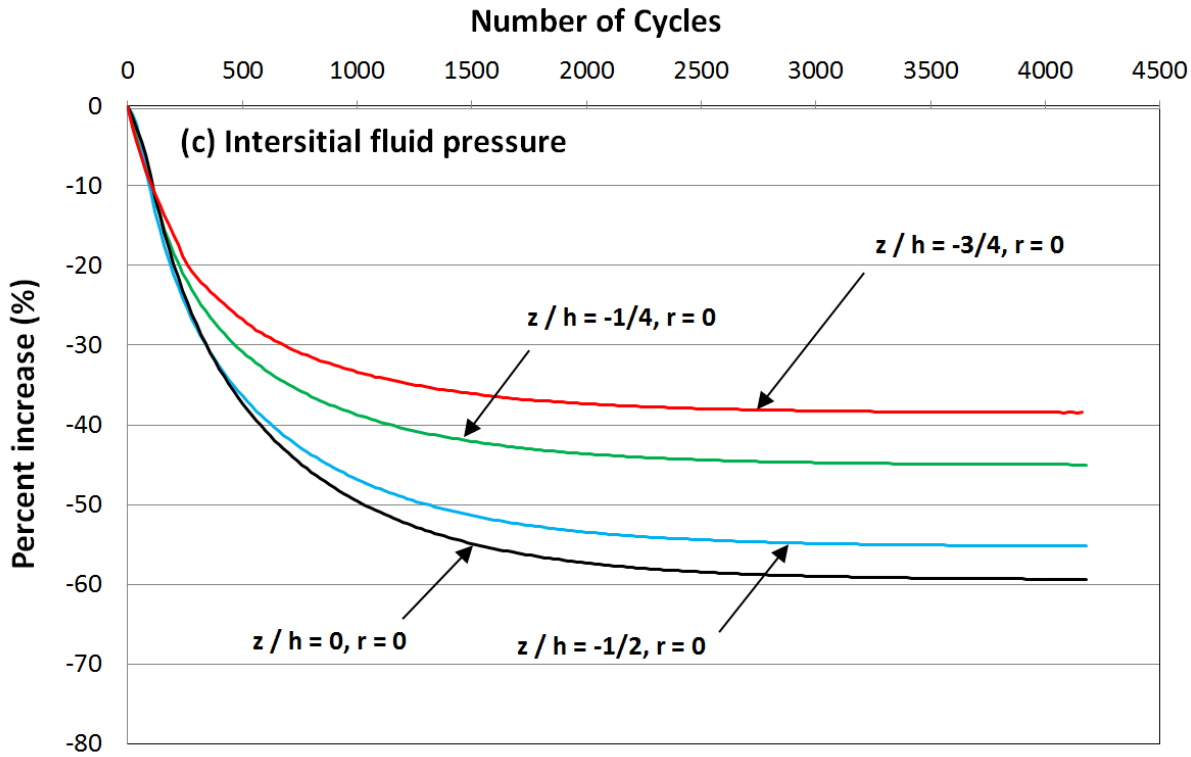

Figure 5 Depth dependent percent increase in the maximum: (a) aggrecan volume fraction, (b) aggregate modulus (H_{-A}), and (c) interstitial fluid pressure, for different number of loading cycles (Specimen A_LPS). The time-dependent percent increase is calculated by using the maximum aggrecan volume fraction, aggregate modulus and interstitial fluid pressure in first loading cycle as the reference value. The duration of one loading cycle = 1s.

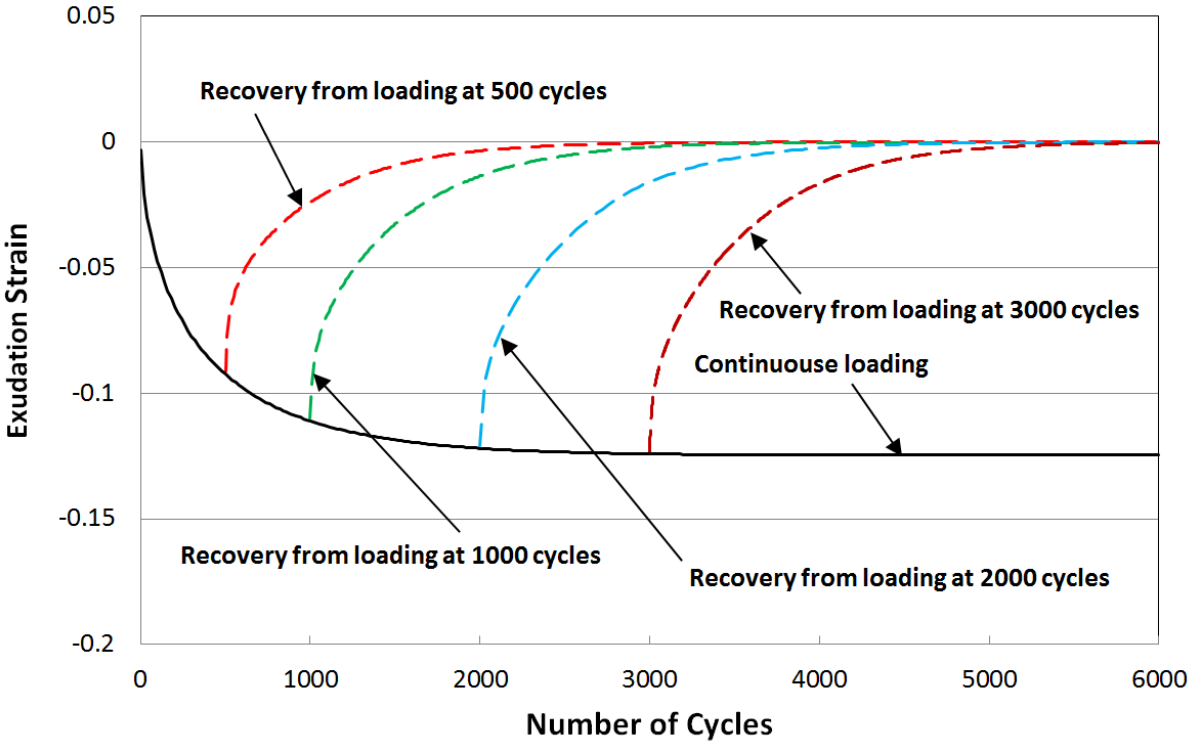

Figure 6 Time-dependent exudation strain profiles when applied cyclic loading is removed after different loading cycles (Specimen A_LPS). The duration of one loading cycle = 1s.

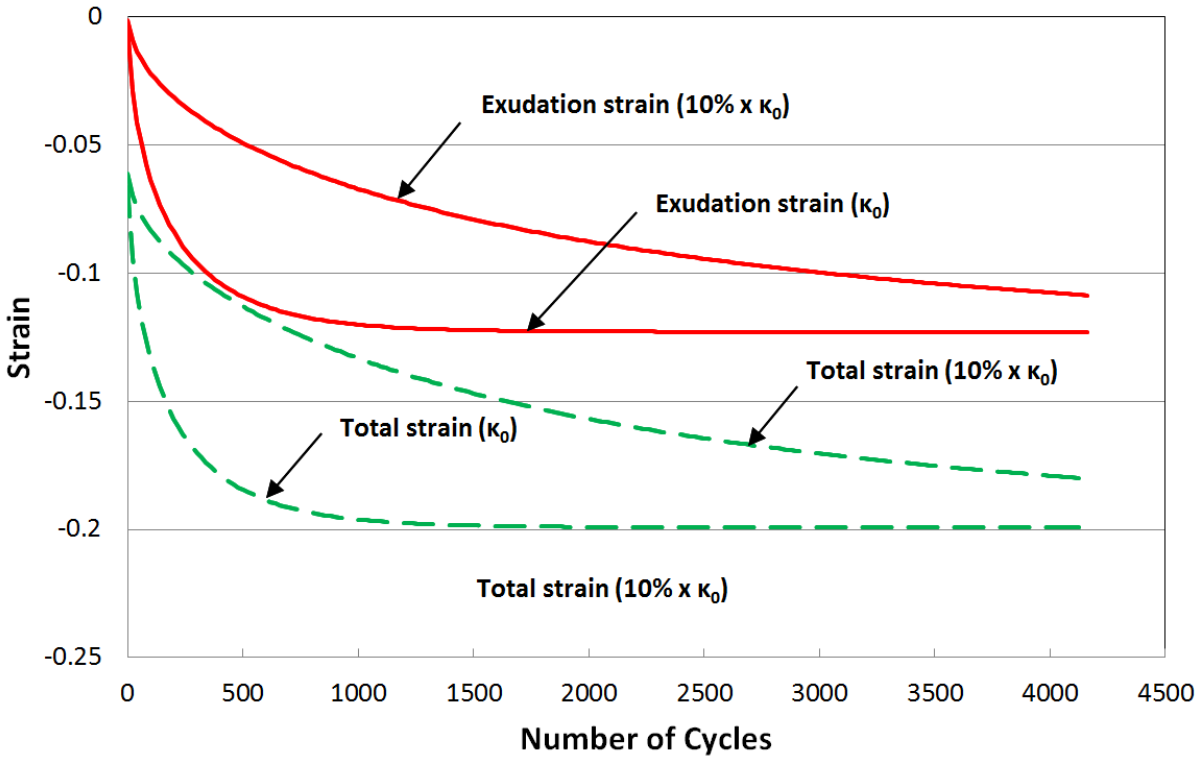

Figure 7 The effects of permeability on time dependent total and exudation strains respectively (Specimen A_LPS). κ_0 is initial cartilage permeability which depends on the initial aggrecan volume fraction. The duration of one loading cycle = 1s.

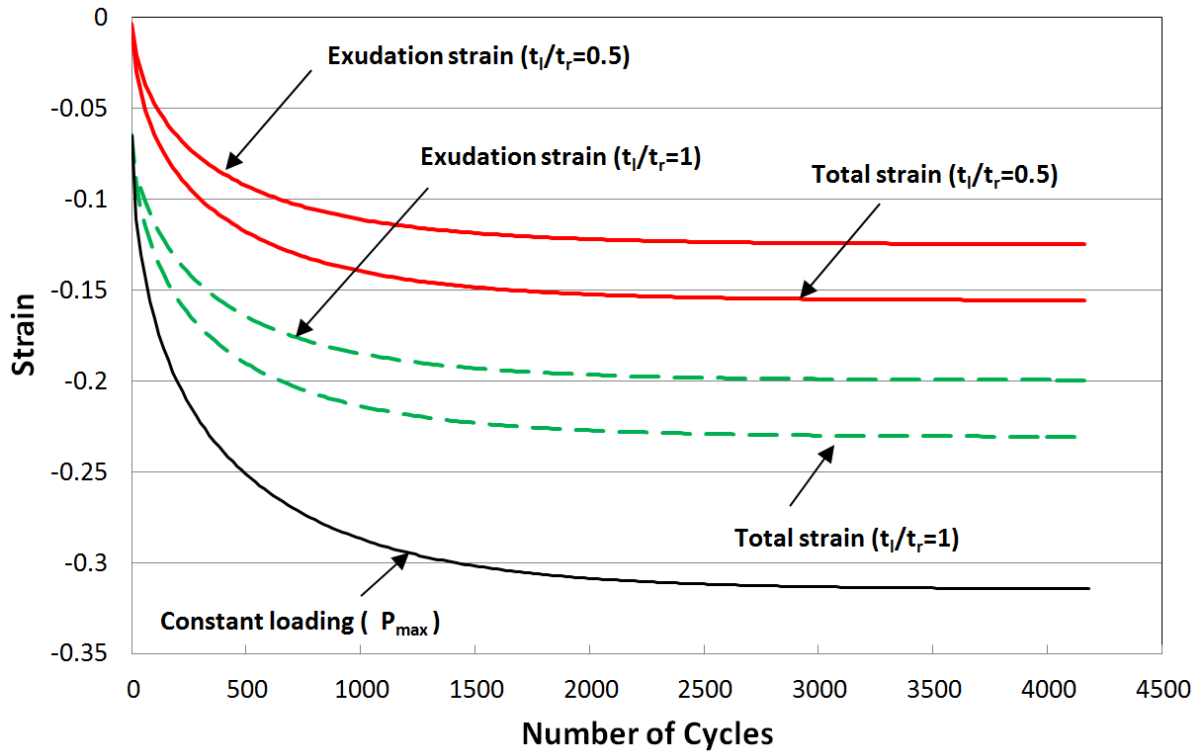

Figure 8 The effects of loading-to-recovery ratio (t_l / t_R) on time dependent total and exudation strains respectively. The magnitude of the constant load = P_{max} = 1.4MPa. The duration of one loading cycle = 1s and t_{l0} = 20ms (Specimen A_LPS).